SCIENTIFIC REPORTS

OPEN

SUBJECT AREAS:

TOPOLOGICAL INSULATORS

ELECTRONIC PROPERTIES AND MATERIALS

Received
20 January 2014

Accepted
14 May 2014

Published
30 May 2014

Correspondence and requests for materials should be addressed to W.-M.L. (wliu@iphy.ac.cn)

The d-p band-inversion topological insulator in bismuth-based skutterudites

Ming Yang & Wu-Ming Liu

Beijing National Laboratory for Condensed Matter Physics, Institute of Physics, Chinese Academy of Sciences, Beijing 100190, China.

Skutterudites, a class of materials with cage-like crystal structure which have received considerable research interest in recent years, are the breeding ground of several unusual phenomena such as heavy fermion superconductivity, exciton-mediated superconducting state and Weyl fermions. Here, we predict a new topological insulator in bismuth-based skutterudites, in which the bands involved in the topological band-inversion process are d- and p-orbitals, which is distinctive with usual topological insulators, for instance in Bi_2Se_3 and BiTeI the bands involved in the topological band-inversion process are only p-orbitals. Due to the present of large d-electronic states, the electronic interaction in this topological insulator is much stronger than that in other conventional topological insulators. The stability of the new material is verified by binding energy calculation, phonon modes analysis, and the finite temperature molecular dynamics simulations. This new material can provide nearly zero-resistivity signal current for devices and is expected to be applied in spintronics devices.

Topological insulator (TI) is a new kind of material which has gapped bulk state and gapless surface state with the latter protected by the topological character of TI[1–10]. For TIs with conserved spin along quantized axis, the topological order parameter is spin Chern number, and TI under time reversal symmetry is characterized by Z_2 quantum number[6]. The unique features of its surface state make TI have potential applications in spintronics and quantum information devices. TI is also the breeding ground for a good number of interesting quantum phenomena such as quantum anomalous Hall effect[11–14], Majorana fermions[15,16] and topological magnetoelectric effect[4]. TIs usually appear in those materials containing elements with strong spin-orbit coupling, for example, the bismuth element in Bi_2Se_3[5,17], BiTeI[18,19], and ScPtBi[3]. Moreover, pressure and strain has been demonstrated as an effective way to modulate the topological property of materials. For instance, $CdSnAs_2$ under a 7% decrease in the lattice constant will become topological insulator[20] while a 6% change in the length of c-axis will drive Bi_2Se_3 from topological non-trivial phase into topological trivial phase[21]. However, more interesting phenomena only can be induced by strong electronic interaction, such as the transition in correlated Dirac fermions[23] and interaction induced topological Fermi liquids[24]. Consequently, those TIs beyond p-band inversion arouse intensive research interest[25–28]. Here, we predict a new d-p band-inversion topological insulator in bismuth-based skutterudites in which the bands involved in the topological band-inversion process are d- and p-orbitals. Due to the present of large d-electronic states, the electronic interaction in this topological insulator is much stronger than that in other conventional topological insulators[27–32].

Skutterudites, such as $RhAs_3$, $IrAs_3$, $IrSb_3$ and IrP_3, crystallize in a cage-like crystal structure in which each transition metal atom octahedrally coordinates to six pnictide atoms[33,34] (see Fig. 1 (a) where $IrBi_3$ is illustrated). They have large Seebeck coefficients and therefore can behave as excellent thermoelectric materials[44]. The discovery of heavy fermion superconductivity[45], exciton-mediated superconducting state[46] and Weyl fermions[47] in this system makes skutterudites a hot spot in condensed matter physics. Besides those skutterudites naturally exist, a number of new members in skutterudites have been experimentally synthesized, such as $NiSb_3$[48] in 2002 and $RuSb_3$[34] in 2004. However, those materials are composed of elements with relatively weak spin-orbit coupling (SOC). Knowing that topological insulators are usually those materials containing elements with strong spin-orbit coupling strength, such as the bismuth element in topological insulator Bi_2Se_3[5,17], BiTeI[18,19] and LaPtBi[22], It is reasonable to ask whether or not skutterudites composed of elements with strong spin-orbit coupling strength, i.e. bismuth, can exist stably and whether they can be topologically non-trivial? This new topological insulator in bismuth-based skutterudites, is exactly such kind of skutterudite material which is able to exist stably, contains elements with strong SOC, and has controllable topological phase transition.

In this work, we predict a new d-p band inversion topological insulator in bismuth-based skutterudites, which is distinctive from usual topological insulators, for instance in Bi_2Se_3 and BiTeI the bands involved in the

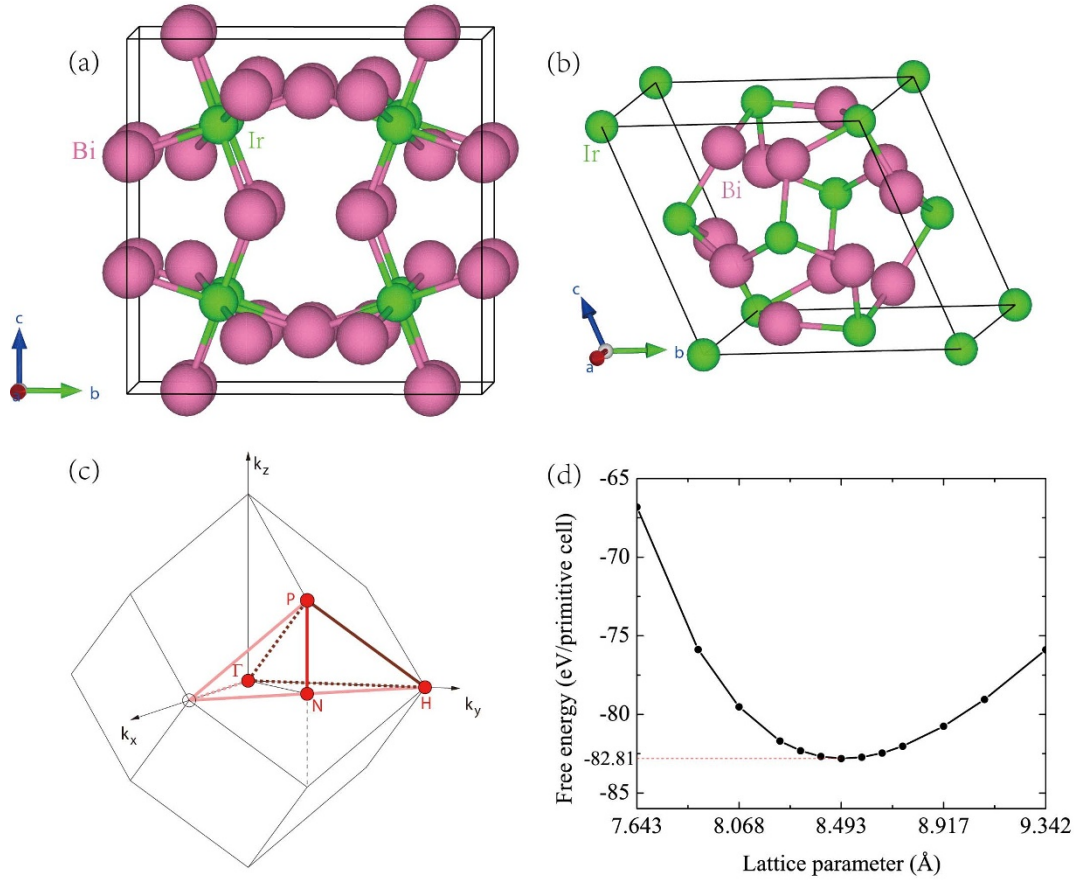

Figure 1 | Crystal structure and Brillouin zone. (a) unit cell of $IrBi_3$, including 8 Ir atoms (green) and 24 Bi atoms (pink). Each Ir atom is surrounded by 6 Bi atoms and each Bi atom has 2 Ir nearest neighbors. (b) The equivalent primitive cell of $IrBi_3$, containing 4 Ir (green) atoms and 12 Bi atoms (pink). (c) The corresponding Brillouin zone and high symmetric points with Γ (0,0,0), H (0,1/2,0), N (1/4,1/4,0), P (1/4,1/4,1/4). (d) Free energy as a function of lattice constant.

topological band-inversion process are only p-orbitals. Due to the present of large d-electronic states, the electronic interaction in this topological insulator is much stronger than that in other conventional topological insulators. The stability of the new material is verified by binding energy calculation, phonon modes analysis, and the finite temperature molecular dynamics (FTMD) simulations. We demonstrate that external strains are able to induce a topological phase transition in this system via band structure calculations. We confirm its topological non-trivial property by Z_2 quantum number calculation.

Results

Crystal structure and optimized lattice parameter. The bismuth-based skutterudite $IrBi_3$ investigated here has space group $IM\bar{3}$, and its crystal structure is shown in Fig. 1. There are 8 Ir atoms and 24 Bi atoms in a unit cell. Each Ir atom is surrounded by 6 Bi atoms and each Bi atom has 2 Ir nearest neighbors (see Fig. 1 (a)). The structure has space inversion symmetry with the inversion center (1/2,1/2,1/2). The structure belongs to the body-centered lattice type, and its primitive cell (Fig. 1 (b)) has a half volume of the unit cell. Fig. 1 (c) shows the Brillouin zone and high symmetric points with Γ (0,0,0), H (0,1/2,0), N (1/4,1/4,0), P (1/4,1/4,1/4).

We first optimize the lattice parameter and ionic positions. The calculated total free energy (solid line) as a function of lattice parameter is shown in Fig. 1 (d). It can be clearly seen that the optimized lattice parameter (corresponding to the position of free energy minimum) of the primitive cell is 8.493Å. This value is 6% larger than that of $IrSb_3$[52], which can be explained that Bi atom has a larger atomic radius than Sb atom.

Binding energy calculation, phonon modes analysis and the finite temperature molecular dynamics simulations. In order to verify the stability of the new material, the authors perform the binding energy calculation, phonon modes analysis and the finite temperature molecular dynamics (FTMD) simulations. The binding energy is calculated by

$$E_b = E_{IrBi_3} - n_{Ir}\cdot E_{Ir} - n_{Bi}\cdot E_{Bi}, \quad (1)$$

where E_{IrBi_3} denotes the free energy of $IrBi_3$ per primitive cell, E_{Ir} and E_{Bi} the free energy of crystalline Ir and Bi per atom, n_{Ir} and n_{Bi} the number of Ir and Bi atoms in $IrBi_3$ primitive cell. By simple calculation [There are $n_{Ir} = 4$ Ir atoms and $n_{Bi} = 12$ Bi atoms in an $IrBi_3$ primitive cell. At GGA level, $E_{Ir} = -8.69$ eV for crystalline Ir with space group $FM\bar{3}M$ and $E_{Bi} = -3.70$ eV for crystalline Bi with space group $IM\bar{3}M$. From Fig. 1(d) we read $E_{IrBi_3} = -82.81$ eV. Substituting the above values in Eq.(1), we arrived at the binding energy $E_b = -3.65$ eV.], E_b is found to be equal to -3.65 eV per primitive cell. The negative value of binding energy infers a stable state of $IrBi_3$.

Fig. 2 shows the phonon dispersion and phonon density of states (DOS) for $IrBi_3$ at zero strain. In the phonon DOS subfigure, the black solid line represents the total phonon density of states, while the green and red shaded areas represent the states coming from Ir and Bi atoms, respectively. Phonon states in the low energy range are mostly composed of states from Bi atoms, indicating that Bi atoms in $IrBi_3$ are much easier to vibrate than the Ir atoms. The phonon dispersion and phonon DOS show no imaginary frequency, indicating that $IrBi_3$ is stable.

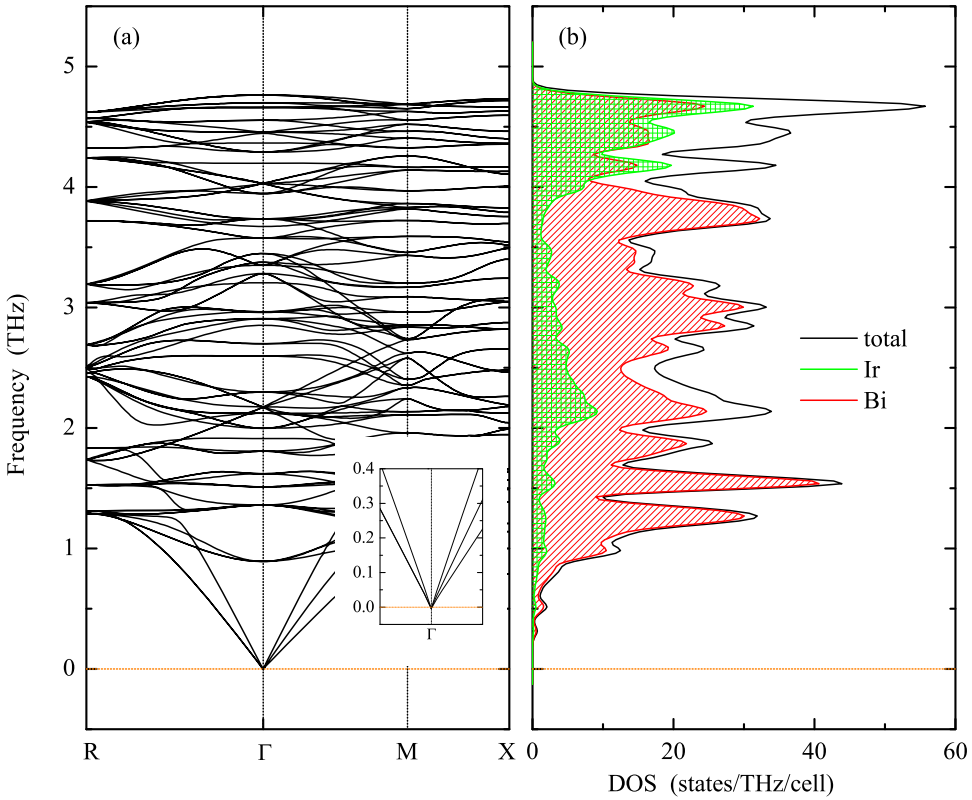

Figure 2 | Phonon dispersion and phonon density of states for $IrBi_3$. Orange dotted lines in all subfigures denotes the zero frequency. Calculations are performed at zero strain. (a) phonon dispersion curves for $IrBi_3$, in which the inset shows the dispersion near the zero energy. (b) phonon density of states for $IrBi_3$, in which black solid line represents the total phonon density of states, while the green and red shaded areas represent the states coming from Ir and Bi atoms, respectively. Phonon states in the low energy range are mostly composed of states of Bi atoms, indicating that Bi atoms in $IrBi_3$ are much easier to vibrate than the Ir atoms. The phonon dispersion and phonon density of states shows no imaginary frequency, indicating that $IrBi_3$ is stable.

In addition, the dynamical stability of the material is further checked by finite temperature molecular dynamics simulations at temperature 300 K for room temperature and 30 K for low temperature. During the simulations, a $2 \times 2 \times 2$ supercell containing 256 atoms is used. The length of time-step is chosen as 5 fs and simulations with 1000 steps are executed. It is observed that, the atoms shake around the equilibrium positions back and forth while the extent of such motion under 300 K is larger than under 30 K (the evolution of atomic positions can be found in movies in supplementary information). However, no structural collapse happens throughout the simulations, which can also be seen from the free energies curves as the functions of time-step shown in Fig. 3. It is also observed that, the crystal structure always remains nearly the same as the initial crystal structure. Actually, as is shown in the inset of Fig. 3, the crystal structure corresponding to the last free energy maximum in T = 300 K case (right), still shows no significant structural differences as compared with the initial crystal structure (left). The lattice relaxation, binding energy calculation, phonon modes analysis together with FTMD simulations mentioned above provide an authentic test for the stability of bismuth-based skutterudite $IrBi_3$.

Strain-induced d-p band-inversion topological insulator. The calculated band structures are listed in Fig. 4, where the black and blue lines represent the GGA and GGA+U band structures, respectively. As is shown in Fig. 4 (a), before exerting pressure, $IrBi_3$ resides in the normal metal state with its bands crossing the Fermi level several times. Subfigure (b) to (d) represent the band structures at isotropic strain 3%, 6%, 9% respectively. With the increase of isotropic strain ((a) to (d)), the valence band crossing the E_F along H-N moves downwards and the density of states (DOS) at Fermi level decreases gradually. Under a 9% isotropic strain, the bands go across the Fermi level at Γ point but not at other points in Brillouin Zone (BZ) (see Fig. 4 (d)), and the conduction band minimum and valence band maximum degenerate so that the material behaves as a semi-metal which have a zero energy gap, just like Graphene and $CeOs_4As_{12}$[8]. This degeneracy at Γ is protected by the cubic symmetry of crystal, which, as is tested by us, cannot be eliminated by small changes of the lattice constant. In order to shift the degeneracy at Γ, one needs to break that symmetry. An unsophisticated way is to add an anisotropy just like what was done on $CdSnAs_2$[20]. Here, we simply further impose a 2% suppression on the c-axis of the primitive cell while remaining the length of a- and b-axis unchanged, which imposes anisotropy on the system. While the anisotropy does not change the parities of each band, it opens a gap at the Fermi level, dragging the system in the insulating state (see Fig. 4 (e)). Fig. 4 (f) shows the Ir-d projected band structure near the Fermi level and near Γ point, in which the radii of red circles correspond to the proportion of Ir-d electrons. It can be seen that, those localized bands above the Fermi level are mainly contributed by d-orbitals of Ir atoms. The highly dispersive band below the Fermi level is mainly contributed by p-orbitals of Bi atoms, and it has little weight of Ir atoms in those k-points far away from Γ point. However, in the vicinity of Γ point, the weight of Ir atoms in that band increases rapidly and becomes dominating orbital component, showing an apparent band inversion. Such band-inversion character is further checked by the modified Becke-Johnson (mBJ) potential (see supplementary information), which is proved to be able to predict an accurate band gap and band order[53–55]. In order to further confirm the topological property in such condition, we calculate the Z_2 topological

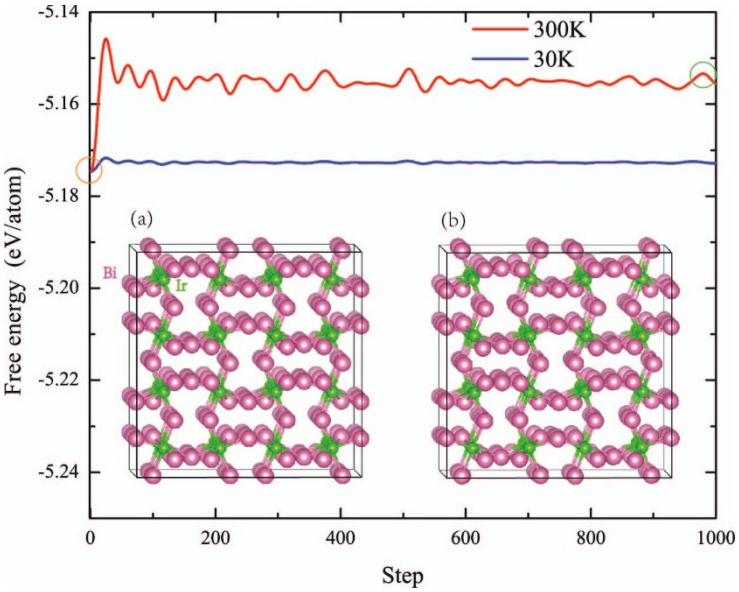

Figure 3 | Finite temperature molecular dynamics. Free energies as functions of time-step at temperature T = 30 K (blue curve) and T = 300 K (red curve). The slight shift of the free energy curves corresponds to the oscillations of each atom around their equilibrium position. The absence of sharp changes in such curves indicates that no structural phase-transition happens throughout the whole simulation process. The initial crystal structure (denoted by the orange circle on the free energy curve) is plotted in inset (a). The crystal structure corresponding to the last free energy maximum (denoted by the green circle on the free energy curve) is shown in inset (b) as a comparison. It can be seen that, the latter still shows no significant structural differences as compared with the initial crystal structure.

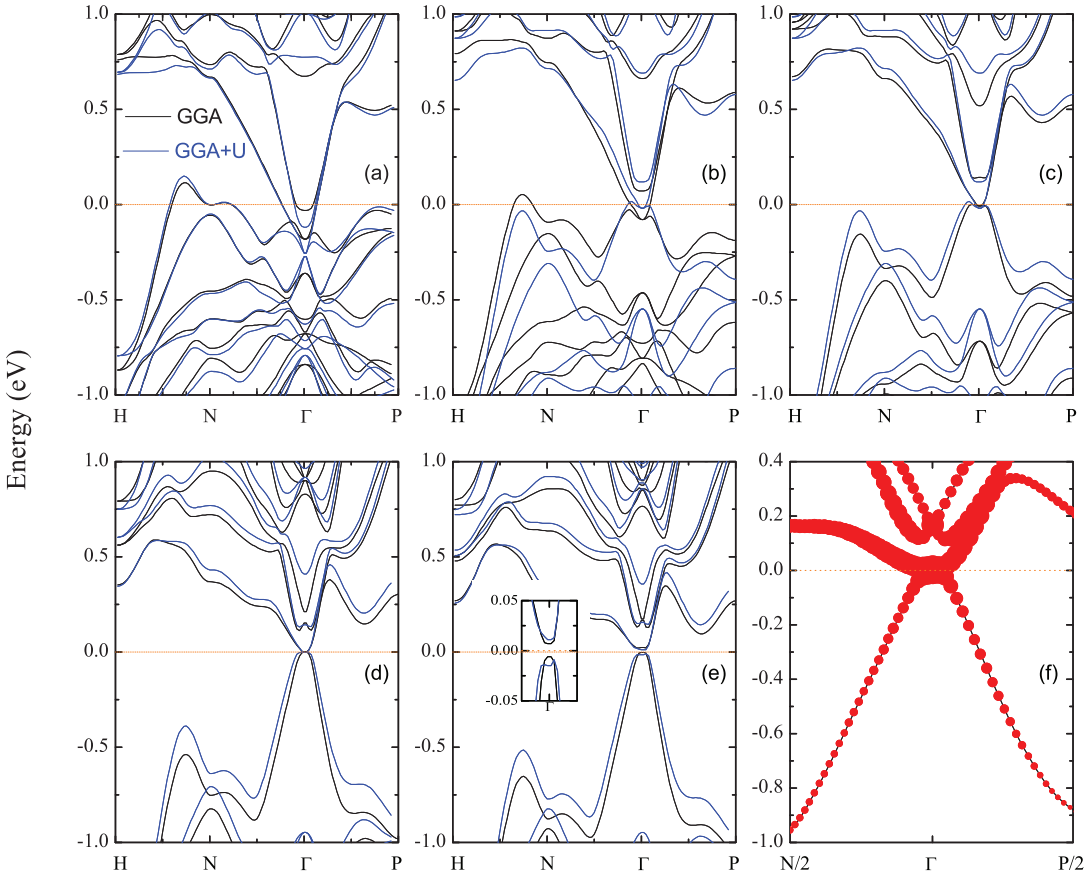

Figure 4 | Band structures of $IrBi_3$. The black and blue lines in all subfigures represent the GGA band structures and GGA+U band structures respectively. (a) band structure without exerting pressure, the system is in normal metal state with its bands go across the Fermi level several times. (b) to (d) represent the band structures at isotropic strain 3%, 6%, 9% respectively. With the increase of isotropic strain ((a) to (d)), the valence band crossing the E_F along H-N moves downwards gradually. In the band structure under 9% uniform strain (d), a zero gap metal state is obtained. (e) further impose a 2% suppression on the length of c-axis of the primitive cell, a gap appeared at the Fermi level due to the breaking of the cubic symmetry. The inset of (e) is the zoom-in of the band structure close to the Fermi level. (f) Ir-d projected band structure near Fermi level, the radii of red circles are proportional to the weight of Ir-d states, showing a significant band inversion.

Table 1 | Parities of top-most isolated valence bands at eight time-reversal invariant momenta. Positive parity is denoted by + while negative denoted by −. Products of the occupied bands at each time-reversal invariant momentum are listed in the right-most column. As is shown, the product of parities of occupied bands contributes a −1 at (0,0,0) while +1 at the seven other time-reversal invariant momenta, resulting in $\nu_0 = 1$, $\nu_1 = \nu_2 = \nu_3 = 0$

(0,0,0)	+ + + + + + + + − + − − + + + + + + + − − − + + + − − + + − + − − +	−
(π,0,0)	− + − + − + − + − + + − − + − + − + + − − + − + − + − + − − + + − + −	+
(0,π,0)	+ − + − − + + − − + + − − + − + − + + − − + − + − + − − + + − − + − +	+
(0,0,π)	− + − + + − − + + − − + − + − + + − − + + − + − + − + + − − + + − + −	+
(π,π,0)	+ − + − − + + − + − − + + − + − + − − + + − + − + − + − − + + − − + +	+
(π,0,π)	− + − + − + − + − + + − − + − + − + + − − + − + − + − + − − + + − + −	+
(0,π,π)	+ − + − − + + − + − − + + − + − + − − + + − + − + − + − − + + − + − − +	+
(π,π,π)	+ + + + + + + − + + − − + + + − + + − + − + + − + − − + + + − − + −	+

quantum number of the system by the Fu-Kane method[6]. The index for strong topological insulators ν_0 is expressed as $(-1)^{\nu_0} = \Pi_{i=1}^{8} \delta_i$ in which $\delta_i = \Pi_{m=1}^{N} \xi_{2m}(\Gamma_i)$ represents the product of the parities of the occupied band at 8 time-reversal invariant momenta Γ_i. The calculated parities of top-most isolated valence bands (here refers to the isolated block of states between −8.0 eV to 0 eV in Fig. 5) at eight time-reversal invariant momenta are listed in Table 1, where the deeper states (those states lower than −9.5 eV in Fig. 5) separated far from top-most isolated valence bands are ignored because they don't change system's band topology. As is shown, the product of parities of occupied bands contributes a −1 at Γ while +1 at the seven other time-reversal invariant momenta. As a result, Z_2 quantum number is $\nu_0 = 1$, $\nu_1 = \nu_2 = \nu_3 = 0$, which corresponds to a strong topological insulator.

Partial-density of states and the d-p orbitals dominating property near the Fermi level. Fig. 5 depicts the atomic- and orbital-resolved density of states (DOS). The black solid lines in subfigure (a)(b)(c) represent the total DOS. Fig. 5 (a) is atomic-resolved DOS, in which the green curve represents the states of Ir while the red curve represents the states of Bi. It's clear that the DOS of both types of atoms is in quite large values, indicating that both types of atoms make a significant contribution to the total DOS. This is different from MoS_2 where states near Fermi level are dominated by only one kind of atom (Mo)[56]. Fig. 5 (b) and (c) are orbital-resolved DOS of Ir and Bi atoms, respectively. Green, blue and red curves represent s-, p- and d-orbitals. One character of the material introduced here is a large proportion of d-states near E_F.

Further, we calculate the d-orbitals projected band structures (see Fig. 6) in the local coordinate of the Bi octahedral. The orange, violet, red, green and blue colors in Fig. 6 represent the d_{z^2}, $d_{x^2-y^2}$, d_{xy}, d_{yz} and d_{xz} orbitals respectively. The radii of circles are proportional to the weights of corresponding orbitals. It can be seen that, the t_{2g} orbitals (including the d_{xy}, d_{yz} and d_{xz} orbitals) reside far below the Fermi level and are fully occupied. While, the lowest three conduction bands are mainly contributed by the e_g orbitals (including the d_{z^2} and $d_{x^2-y^2}$ orbitals). More specifically, the $d_{x^2-y^2}$ orbital makes an even larger contribution than the the d_{z^2} orbital for the lowest conduction band. The large proportion of d-states near E_F is distinctively different from usual TI materials, for example states near E_F mainly containing s-p electrons in HgTe and p-electrons in Bi_2Se_3. The large proportion of d-states near E_F indicates that electrons in such material process strong electronic correlations and are more localized than other TI materials. The strong electronic correlations make the material a good platform for investigating the effect of correlations on the topology, as well as a candidate for realizing the quantum information device based on correlations. The localization will enhance the effective mass of bulk electrons, and hence reduce the bulk contribution to the local current at finite temperature, making the spin-binding property more apparent, which is helpful in fabricating spintronics devices with higher stability.

Discussion

Experimentally, the new strain-induced topological insulator $IrBi_3$ could be grown using the Bridgman method, by which the CoP_3[33] and the $RuSb_3$[34] crystals have been successfully synthesized. The

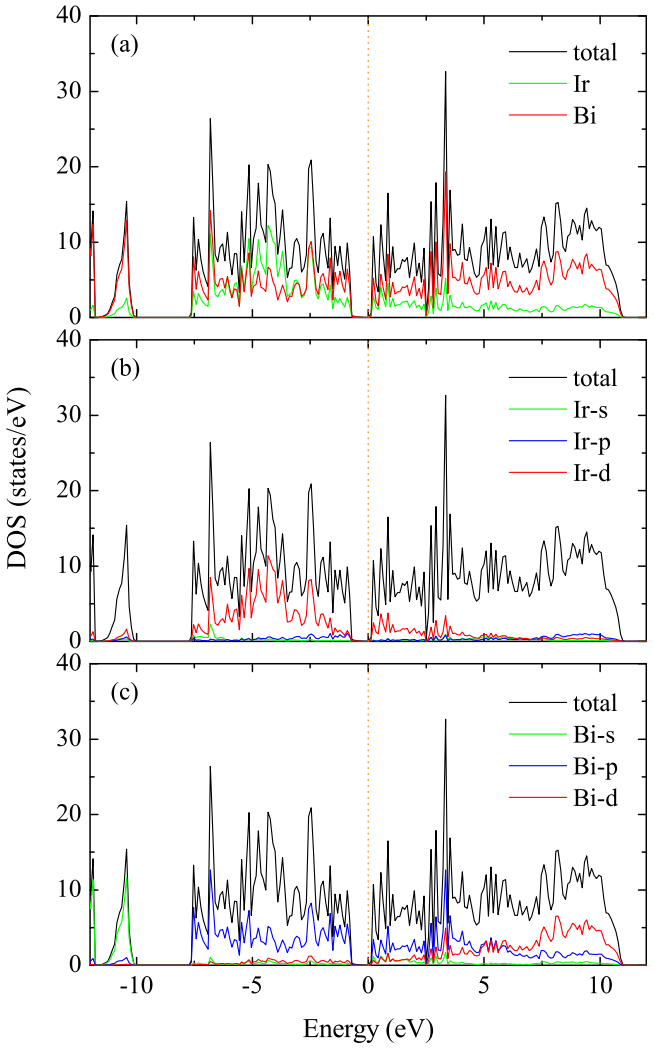

Figure 5 | The atomic- and orbital-resolved density of states. The black solid lines in all subfigures represent the total density of states (DOS). (a) atomic-resolved DOS, in which the green curve represents the states of Ir and the red curve represents the states of Bi. It's clear that both type of atom made a significant contribution to the total DOS, different from MoS_2 where states near Fermi level are dominated by Mo. (b) and (c) are orbital-resolved DOS of Ir and Bi atom respectively. Green, blue and red curves represent s-, p- and d-orbitals.

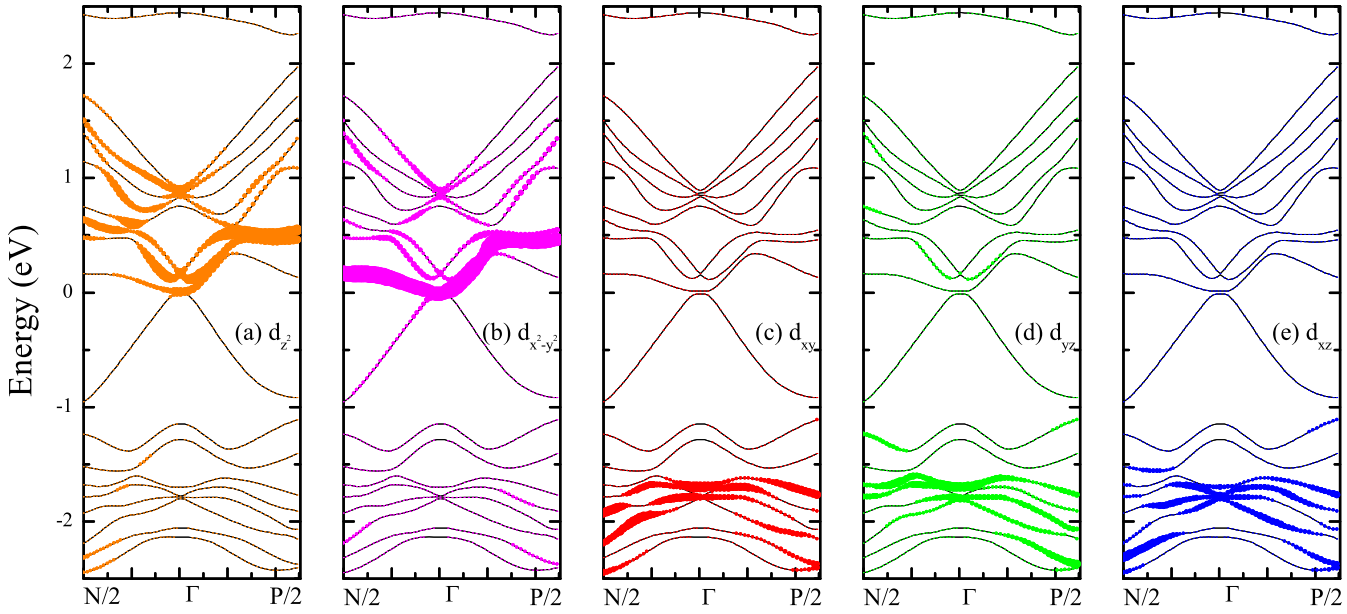

Figure 6 | Orbital-projected band structures. The orange, violet, red, green and blue colors in subfigures represent the d_{z^2}, $d_{x^2-y^2}$ and d_{xy}, d_{yz} and d_{xz} orbitals respectively. The radii of circles are proportional to the weights of corresponding orbitals. The Fermi level is set to be zero energy. It can be seen that, the t_{2g} orbitals (including the d_{xy}, d_{yz} and d_{xz} orbitals) reside far below the Fermi level and are fully occupied. While, the lowest three conduction bands are mainly contributed by the e_g orbitals (including the d_{z^2} and $d_{x^2-y^2}$ orbitals). More specifically, the $d_{x^2-y^2}$ orbital makes an even larger contribution than the the d_{z^2} orbital for the lowest conduction band.

crystal growth should be conducted in a sealed quartz ampoule. The iridium and bismuth should be coated by graphite and then introduced into the quartz ampoule. A temperature gradient of about 50°C/cm should be maintained at the growth interface, just like in the case of $RhSb_3$[35]. To remove the excess bismuth in the as-grown crystal, post-annealing should be performed[36]. After the synthesis of the new material, its crystal structure could be characterized by the X-ray diffraction using the monochromatic Cu Kα radiation[37]. Then, the strains could be generated by a pair of diamond anvils[38], which was used to generate strong pressure even above 200 GPa[39]. Moreover, the real-time pressure strength could be detected by ruby fluorescence method[38,40]. In order to verify the topological property of the material, it is suggested to perform the transport measurements[41]. Similar to Bi_2Se_3, the observation of the spin-Hall current[42] and the non-equally spaced Landau levels[43] in $IrBi_3$ will be signatures of the Dirac fermions in surface of the topological insulator[1].

In this work, we predict a d-p band inversion topological insulator bismuth-based skutterudite $IrBi_3$, and verify its stability. Our results indicate that this material is zero gap semi-metal after imposing uniform strain, and it can become topological insulator if an anisotropy is further applied to break the cubic symmetry. Furthermore, near the Fermi level there is a large proportion of d-electronic states which is distinctive from usual topological insulators, for instance in Bi_2Se_3 and BiTeI the bands involved in the topological band-inversion process are only p-orbitals. Consequently, the electronic interaction in this topological insulator is much stronger than that in other conventional topological insulators. This provides realistic material for investigating the effect of correlations on the topology, fabricating quantum information devices and spintronics devices with higher stability.

Methods

Our first principle calculations are in the framework of the generalized gradient approximation (GGA) of the density functional theory. The VASP package[49,50] has been employed and the projector-augmented-wave pseudo-potentials[51] are used. Plane waves with a kinetic energy cut-off E_c of 400 eV are used as basis sets and k-point grids in Brillouin zone is chosen as $6 \times 6 \times 6$ according to the Monkhorst-Pack scheme. The relaxations are carefully made so that the forces on atoms are smaller than 0.0003 eV/Å, in which the conjugate gradient algorithm is utilised. In the finite temperature molecular dynamics simulations, a $2 \times 2 \times 2$ supercell containing 256 atoms is used and the length of time-step is chosen as 5 fs. The phonon dispersion curve and phonon density of states are obtained using the force-constant method by phonopy code[57]. The effect of spin-orbit coupling (SOC) is included in the calculations after the structural relaxations. GGA+U calculations are based on the Dudarev's approach implemented in VASP, with the effective on site Coulomb interaction parameter $U = 3.0$ eV and the effective on site exchange interaction parameter $J = 0.5$ eV for d-orbitals of Ir atoms[58]. The GGA band structures are checked by the full-potential DFT code WIEN2k[59] in the supplementary information. We also use the modified Becke-Johnson (mBJ) semilocal exchange-correlation potential[53,54] to further check the band order and the magnitude of energy gap, and in this process the GGA wave function is used to initialize the mBJ calculation.

1. Bernevig, B. A., Hughes, T. A. & Zhang, S. C. Quantum spin Hall effect and topological phase transition in HgTe quantum wells. *Science* **314**, 1757 (2006).
2. Lin, H., Wray, L. A., Xia, Y., Xu, S. Y., Jia, S., Cava, R. J., Bansil, A. & Hasan, M. Z. Half-Heusler ternary compounds as new multifunctional experimental platforms for topological quantum phenomena. *Nat. Mat.* **9**, 546 (2010).
3. Chadov, S., Qi, X. L., Kubler, J., Fecher, G. H., Felser, C. & Zhang, S. C. Tunable multifunctional topological insulators in ternary Heusler compounds. *Nat. Mat.* **9**, 541 (2010).
4. Qi, X. L., Hughes, T. L. & Zhang, S. C. Topological field theory of time-reversal invariant insulators. *Phys. Rev. B* **78**, 195424 (2008).
5. Zhang, H. J., Liu, C. X., Qi, X. L., Dai, X., Fang, Z. & Zhang, S. C. Topological insulators in Bi2Se3, Bi2Te3 and Sb2Te3 with a single Dirac cone on the surface. *Nat. Phys.* **5**, 438 (2009).
6. Fu, L. & Kane, C. L. Topological insulators with inversion symmetry. *Phys. Rev. B* **76**, 045302 (2007).
7. Xia, Y. *et al.* Observation of a large-gap topological-insulator class with a single Dirac cone on the surface. *Nat. Phys.* **5**, 398 (2009).
8. Yan, B. H., Muchler, L., Qi, X. L., Zhang, S. C. & Felser, C. Topological insulators in filled skutterudites. *Phys. Rev. B* **85**, 165125 (2012).
9. Liu, C. C., Feng, W. X. & Yao, Y. G. Quantum spin Hall effect in silicene and two-dimensional germanium. *Phys. Rev. Lett.* **107**, 076802 (2011).
10. Sun, F. D., Yu, X. L., Ye, J. W., Fan, H. & Liu, W. M. Topological quantum phase transition in synthetic non-abelian gauge potential: gauge invariance and experimental detections. *Sci. Rep.* **3**, 2119 (2013).
11. Yu, R., Zhang, W., Zhang, H. J., Zhang, S. C., Dai, X. & Fang, Z. Quantized anomalous Hall effect in magnetic topological insulators. *Science* **329**, 61 (2010).
12. Qiao, Z. H., Tse, W., Jiang, H., Yao, Y. G. & Niu, Q. Two-Dimensional topological insulator state and topological phase transition in bilayer graphene. *Phys. Rev. Lett.* **107**, 256801 (2011).
13. Zhang, X. L., Liu, L. F. & Liu, W. M. Quantum anomalous Hall effect and tunable topological states in 3d transition metals doped silicene. *Sci. Rep.* **3**, 2908 (2013).
14. Zhang, J. M., Zhu, W. G., Zhang, Y., Xiao, D. & Yao, Y. G. Tailoring magnetic doping in the topological insulator Bi2Se3. *Phys. Rev. Lett.* **109**, 266405 (2012).

15. Fu, L. & Kane, C. L. Superconducting proximity effect and Majorana fermions at the surface of a topological insulator. *Phys. Rev. Lett.* **100**, 096407 (2008).
16. Tiwari, R. P., Zlicke, U. & Bruder, U. Majorana fermions from Landau quantization in a superconductor and topological-insulator hybrid structure. *Phys. Rev. Lett.* **110**, 186805 (2013).
17. Zhang, W., Yu, R., Zhang, H. J., Dai, X. & Fang, Z. First-principles studies of the three-dimensional strong topological insulators Bi2Te3, Bi2Se3 and Sb2Te3. *New Journal of Physics* **12**, 065013 (2010).
18. Bahramy, M. S., Yang, B. J., Arita, R. & Nagaosa, N. Emergent quantum confinement at topological insulator surfaces. *Nat. Commun.* **3**, 679 (2012).
19. Wang, C. R. *et al*. Magnetotransport in copper-doped noncentrosymmetric BiTeI. *Phys. Rev. B* **88**, 081104(R) (2013).
20. Feng, W. X., Xiao, D., Ding, J. & Yao, Y. G. Three-dimensional topological insulators in I-III-VI2 and II-IV-V2 chalcopyrite semiconductors. *Phys. Rev. Lett.* **106**, 016402 (2011).
21. Liu, W. L. *et al*. Anisotropic interactions and strain-induced topological phase transition in Sb2Se3 and Bi2Se3. *Phys. Rev. B* **84**, 245105 (2011).
22. Xiao, D. *et al*. Half-Heusler compounds as a new class of three-dimensional topological insulators. *Phys. Rev. Lett.* **105**, 096404 (2010).
23. Yu, S. L., Xie, X. C. & Li, J. X. Mott physics and topological phase transition in correlated dirac fermions. *Phys. Rev. Lett.* **107**, 010401 (2011).
24. Castro, E. V. *et al*. Topological fermi liquids from coulomb interactions in the doped honeycomb lattice. *Phys. Rev. Lett.* **107**, 106402 (2011).
25. Doennig, D., Pickett, W. E. & Pentcheva, R. Confinement-driven transitions between topological and Mott phases in (LaNiO3)N/(LaAlO3)M(111) superlattices. *Phys. Rev. B* **89**, 12110(R) (2014).
26. Werner, J. & Assaad, F. F. Interaction-driven transition between topological states in a Kondo insulator. *Phys. Rev. B* **88**, 035113 (2013).
27. Go, A. *et al*. Correlation effects on 3d topological phases: from bulk to boundary. *Phys. Rev. Lett.* **109**, 066401 (2012).
28. Weng, H. M., Zhao, J. Z., Wang, Z. J., Fang, Z. & Dai, X. Topological crystalline Kondo insulator in mixed valence Ytterbium Borides. *Phys. Rev. Lett.* **112**, 016403 (2014).
29. Miyamoto, K. *et al*. Spin-polarized Dirac-cone-like surface state with d character at W(110). *Phys. Rev. Lett.* **108**, 066808 (2012).
30. Kang, C. J. *et al*. Band symmetries of mixed-valence topological insulator: SmB6. *Arxiv* 1312.5898 (2013).
31. Okamoto, S. *et al*. Correlation effects in (111) bilayers of perovskite transition-metal oxides. *Arxiv* 1401.0009 (2014).
32. Chen, G. & Hermele, M. Magnetic orders and topological phases from f-d exchange in pyrochlore iridates. *Phys. Rev. B* **86**, 235129 (2012).
33. Niwa, K. *et al*. Compression behaviors of binary skutterudite CoP3 in noble gases up to 40 GPa at room temperature. *Inorg. Chem.* **50**, 3281 (2011).
34. Smalley, A., Jespersen, M. L. & Johnson, D. C. Synthesis and structural evolution of RuSb3, a new metastable skutterudite compound. *Inorg. Chem.* **43**, 2486 (2004).
35. Caillat, T., Fleurial, J. P. & Borshchevsky, A. Bridgman-solution crystal growth and characterization of the skutterudite compounds CoSb3 and RhSb3. *J. Crystal Growth* **166**, 722 (1996).
36. Akasaka, M. *et al*. Effects of post-annealing on thermoelectric properties of p-type CoSb3 grown by the vertical Bridgman method. *J. Alloys and Compounds* **386**, 228 (2005).
37. Takizawa, H., Miura, K., Ito, M., Suzuki, B. & Endo, T. Atom insertion into the CoSb skutterudite host lattice under high pressure. *J. Alloys and Compounds* **282**, 79 (1999).
38. Xi, X. X. *et al*. Signatures of a pressure-induced topological quantum phase transition in BiTeI. *Phys. Rev. Lett.* **111**, 155701 (2013).
39. Nakamoto, Y. *et al*. Generation of Multi-megabar pressure using nano-polycrystalline diamond anvils. *Jpn. J. App. Phys.* **46**, 640 (2007).
40. Zhu, J. L. *et al*. Superconductivity in topological insulator Sb2Te3 induced by pressure. *Sci. Rep.* **3**, 2016 (2013).
41. Hamlin, J. J. *et al*. High pressure transport properties of the topological insulator Bi2Se3. *J. Phys.: Condens. Matter* **24**, 035602 (2012).
42. Dora, B. & Moessner, R. Dynamics of the spin Hall effect in topological insulators and graphene. *Phys. Rev. B* **83**, 073403 (2011).
43. Cheng, P. *et al*. Landau quantization of topological surface states in Bi2Se3. *Phys. Rev. Lett.* **105**, 076801 (2010).
44. Sales, B. C., Mandrus, D. & Williams, R. K. Filled skutterudite antimonides: a new class of thermoelectric materials. *Science* **272**, 1325 (1996).
45. Seyfarth, G. *et al*. Multiband superconductivity in the heavy fermion compound PrOs4Sb12. *Phys. Rev. Lett.* **95**, 107004 (2005).
46. Matsumoto, M. *et al*. Exciton mediated superconductivity in PrOs4Sb12. *J. Phys. Soc. J.* **73**, 1135 (2004).
47. Smith, J. C., Banerjee, S., Pardo, V. & Pickett, W. E. Dirac point degenerate with massive bands at a topological quantum critical point. *Phys. Rev. Lett.* **106**, 056401 (2011).
48. Williams, J. M. & Johnson, D. C. Synthesis of the new metastable skutterudite compound NiSb3 from modulated elemental reactants. *Inorg. Chem.* **41**, 4127 (2002).
49. Kresse, G. & Furthmuller, J. Efficient iterative schemes for ab initio total-energy calculations using a plane-wave basis set. *Phys. Rev. B* **54**, 11169 (1996).
50. Kresse, G. & Furthmuller, J. Efficiency of ab-initio total energy calculations for metals and semiconductors using a plane-wave basis set. *Comput. Mater. Sci.* **6**, 15 (1996).
51. Blochl, P. E. Projector augmented-wave method. *Phys. Rev. B*, **50**, 17953 (1994).
52. Kjekshus, A. *et al*. Compounds with the skutterudite type crystal structure. III. structural data for arsenides and antimonides. *Acta Chemica Scandinavica* **28**, 99 (1974).
53. Becke, A. & Johnson, E. A simple effective potential for exchange. *J. Chem. Phys.* **124**, 221101 (2006).
54. Tran, F. & Blaha, P. Accurate band gaps of semiconductors and insulators with a semilocal exchange-correlation potential. *Phys. Rev. Lett.* **102**, 226401 (2009).
55. Feng, W. X., Xiao, D., Zhang, Y. & Yao, Y. G. Half-Heusler topological insulators: A first-principles study with the Tran-Blaha modified Becke-Johnson density functional. *Phys. Rev. B* **82**, 235121 (2010).
56. Xiao, D., Liu, G. B., Feng, W. X., Xu, X. D. & Yao, W. Coupled spin and valley physics in monolayers of MoS2 and other group-VI dichalcogenides. *Phys. Rev. Lett.* **108**, 196802 (2012).
57. Togo, A. *et al*. First-principles calculations of the ferroelastic transition between rutile-type and CaCl2-type SiO2 at high pressures. *Phys. Rev. B* **78**, 134106 (2008).
58. Solovyev, I. V. & Dederichs, P. H. Corrected atomic limit in the local-density approximation and the electronic structure of d impurities in Rb. *Phys. Rev. B* **50**, 16861 (1994).
59. Blaha, P., Schwarz, K., Madsen, G., Kvasnicka, D. & Luitz, J. WIEN 2k, Augmented Plane Wave Local Orbitals Program for Calculating Crystal Properties, Vienna, Austria, (2001).

Acknowledgments

We acknowledge helpful discussions with H.M. Weng and X.X. Wu. This work is supported by the NKBRSFC (Grants Nos. 2011CB921502, 2012CB821305), NSFC (grants Nos. 61227902, 61378017). The numerical calculations are performed on the Shenteng supercomputer at CNIC-CAS and on the Dawning cluster at IOP-CAS.

Author contributions

M.Y. performed the numerical calculations. All authors analyzed the data and wrote the manuscript.

Additional information

Supplementary information accompanies this paper at http://www.nature.com/scientificreports

Competing financial interests: The authors declare no competing financial interests.

How to cite this article: Yang, M. & Liu, W.-M. The d-p band-inversion topological insulator in bismuth-based skutterudites. *Sci. Rep.* **4**, 5131; DOI:10.1038/srep05131 (2014).